CSIRO PUBLISHING

Aust. J. Chem. **2015**, *68*, 1237–1248
http://dx.doi.org/10.1071/CH14639

Full Paper

Aromatic Schiff Bases Multiply Substituted with Terminal Ethynyl Groups: Potential Building Blocks for Conjugated Polymers and Oligomers

Sabina Stahlová,[A] *Jan Sedláček,*[A] *Jan Svoboda,*[A] *Miroslav Polášek,*[B] *and Jiří Zedník*[A,C]

[A]Department of Physical and Macromolecular Chemistry, Faculty of Science, Charles University in Prague, Hlavova 2030, CZ-128 43 Prague 2, Czech Republic.
[B]J. Heyrovský Institute of Physical Chemistry, v.v.i., Academy of Sciences of the Czech Republic, Dolejškova 3, 182 23 Prague 8, Czech Republic.
[C]Corresponding author. Email: jiri.zednik@natur.cuni.cz

Nine mostly novel aromatic Schiff bases containing from two-to-four terminal ethynyl groups and one or two methanimine groups per one molecule are reported. The spectral and density functional theory characteristics and the extent of conjugation are discussed in connection with the structure and architecture of the prepared compounds. The applicability of compounds as building blocks for conjugated polymers is shown in $TaCl_5$-catalyzed polycyclotrimerization (proceeding in ethynyl groups) yielding either soluble luminescent or insoluble microporous polymers.

Manuscript received: 28 October 2014.
Manuscript accepted: 17 December 2014.
Published online: 31 March 2015.

Introduction

Arenes substituted with several terminal ethynyl groups (referred to here as multiethynylarene, MEA) are excellent building blocks (monomers) for the synthesis of conjugated polymers and oligomers of various structures, architectures, and functions.[1–9] The number of ethynyl groups per one MEA molecule (i.e. the monomer functionality, f) ranges mostly from two to four. Various synthetic paths from MEAs to conjugated polymers are described in the literature. Homocoupling of diethynylarenes leads to linear poly(arylenebutadiynylene)s.[1,10] Cross-coupling of diethynylarenes with dibromo- or diiodoarenes provides linear poly(aryleneethynylene)s chain length and end-capping of which can be controlled by composition of the polymerization feed.[4,7,11] Linear polymers are also obtained via Huisgen cycloaddition from diethynylarenes and diazidoarenes.[1] The polycyclotrimerization of mixtures of diethynylarene and alkylacetylene catalyzed by $TaCl_5$ provides soluble hyperbranched polyarylenes and oligoarylenes in which the original arene cores of the monomer molecules are interconnected by benzenetriyl linkers formed via cyclotrimerization of three ethynyl groups.[1,2,12] The soluble branched polymers have also been obtained via chain-growth polymerization from a diethynylarene and monoethynylarene feed (polyacetylene-type polymers).[13,14] The luminescence, response to stimuli, molecular recognition, and other properties are studied on soluble MEA-derived polymers.[1] If MEAs of a higher functionality are polymerized by the above approaches, the insoluble highly cross-linked conjugated networks are obtained. MEAs and corresponding halo- or azidoarenes of an average functionality from 2.5 to 4 are used in the step-growth synthesis of the networks.[8,15–17] The functionality $f = 2$ is reliably sufficient to achieve (hyper)cross-linked networks via polycyclotrimerization[18,19] and chain-growth polymerization[9,20] of MEAs, although in this case, MEAs with $f > 2$ are also sometimes used.[18,21] The networks derived from MEAs are investigated for their optoactive properties,[22,23] porosity, and corresponding applicability in catalysis and the capture of gases and small molecules.[16,24–26]

Arene cores of MEAs mostly consist of isolated or C–C interconnected aromatics.[1–4,18,19] Besides, MEAs have been reported to contain cores in which two or three arene rings are connected by conjugated ethene-1,2-diyl, ethyne-1,2-diyl or azo linker(s) (e.g. 1,4-bis[(4-ethynylphenyl)ethenyl]benzene and 2,5-bis[(4-ethynylphenyl)ethynyl]thiophene MEAs).[27,28] One may assume that the choice of arene cores of MEAs is limited by the requirement of sufficient solubility of MEA. From this point of view, interconnecting arene rings in the MEA core by methanimine (azomethine) –CH=N– group[29] may be a promising step. This group should (1) decrease the rigidity and (2) slightly increase the polarity of the molecules of MEA. Both of these factors should positively contribute to the solubility of MEA. Moreover, the polymers and oligomers prepared from such MEAs may be suitable for post-polymerization modifications involving reactions in the methanimine group. Only several reports can be found in the literature on the Schiff base-type MEAs. Wei et al.[30] used condensation of 3-ethynylaniline with either 1,4- or 1,3-phthaldehyde and 4-ethynylaniline with 1,4-phthaldehyde and prepared respective positional isomers of 1,1′-(phenylene)bis[*N*-(4-ethynylphenyl)methanimine]s. Monomer 1,1′-(1,4-phenylene)bis[*N*-(4-ethynylphenyl)methanimine]

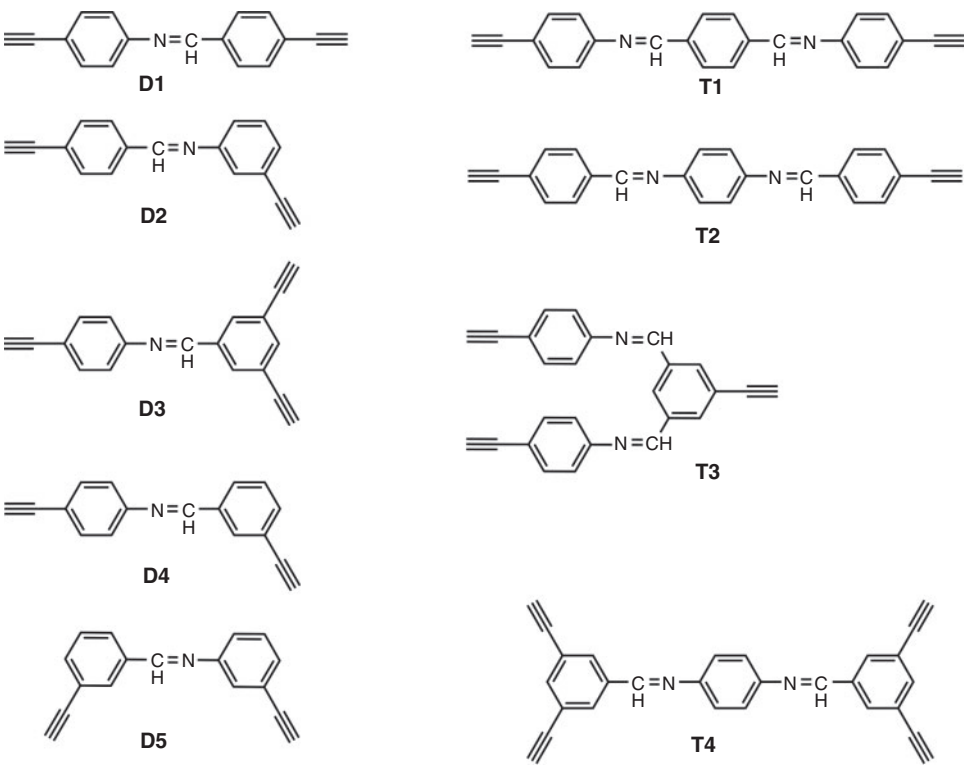

Chart 1. Structure formulae and codes of the prepared MEAs.

was polymerized via Glaser–Hahn oxidative coupling into well-defined –CH=N– groups containing poly(arylenebutadiynylene)-type polymer. Other isomers were applied in the preparation of thermosets via hot-melt processing.[31] 1,1′-(1,4-Phenylene)bis[*N*-(4-ethynylphenyl)methanimine] was also used by Lavastre et al. in a combinatorial chemistry screening in which eight various diethynylarenes were polymerized by Sonogashira cross-coupling with a series of dibromoarenes into (arylene-ethynylene)s.[28] Various monoethynylarenes ($f = 1$) with the methanimine group in the substituent (e.g. *N*-(benzylidene)-4-ethynylanilines and *N*-(4-ethynylbenzylidene)anilines) have also been prepared and characterized.[32,33] With respect to the monofunctionality of these monomers, only the chain-growth mode was possible for their polymerization.[34–37] Linear polyacetylenes containing methanimine groups as parts of the pendant groups were achieved by this approach.

In this contribution, we report the preparation of a series of mostly new MEAs containing in a molecule from two-to-four terminal ethynyl groups on benzene rings interconnected by either one or two methanimine groups. The influence of the molecular structure and architecture (the size of MEA core, positional isomerism on benzene rings, functionality) on the spectral properties and overall conjugation extent of MEAs is discussed on the basis of experimental spectral data and results of density functional theory (DFT) computation. The applicability of the prepared MEAs is demonstrated by $TaCl_5$-catalyzed polymerizations yielding (depending on the conditions) either soluble luminescent or insoluble microporous polycyclotrimers.

Results and Discussion

Synthesis of Schiff Base-Type MEAs

A series of mostly new MEAs with cores containing benzene rings connected by methanimine (azomethine) link(s) have been prepared. Structural formulae, names, and codes of MEAs are given in Chart 1 and the Experimental section. The MEAs were synthesized by one-step condensation from respective amines and aldehydes performed in a minimum amount of methanol at room temperature (Experimental section). The use of the smallest possible amount of methanol was crucial because it supported the precipitation of the products, which are less soluble than the starting amines and aldehydes. The precipitation resulted in a shift in the condensation equilibrium in favour of the product. MEAs were prepared in isolated yields ranging from 62 % to 90 % (see Experimental section); the yield loss is mainly attributed to the purification of the products by their washing with (cold) methanol.

The MEAs with two (ethynyl-substituted) benzene rings connected by one methanimine link are referred to as dimers (D). The functionality, *f*, (i.e. the number of ethynyl groups per one MEA molecule) of the dimer-type MEAs is either 2 (**D1**, **D2**, **D4**, **D5**) or 3 (**D3**). The prepared MEAs containing three benzene rings connected by two methanimine links are referred to as trimers (T). Trimers **T1**, **T2**, and **T4** contain ethynyl groups on terminal benzene rings only (one ethynyl group on each terminal benzene ring, $f = 2$, in **T1** and **T2**, or two ethynyl groups on each terminal benzene ring, $f = 4$, in **T4**). Trimer **T3** has been designed such that each benzene ring (including the central one) bears one ethynyl group ($f = 3$). The ethynyl groups of MEAs are either *para*- or *meta*-positioned with respect to the methanimine group. The compounds **D1**, **T1**, and **T2** possess only *para*-positioned ethynyl groups. Only *meta*-positioned ethynyl groups are present in **D5** and **T4**. The compounds **D2**, **D3**, **D4**, and **T3** contain both *para*- and *meta*-positioned ethynyl groups. Both the *para*- and *meta*- positioning of the ethynyl groups with respect to the methanimine group was realised (particularly in the D series of MEAs) with the aim of evaluating the influence of this positional isomerism on the MEA conjugation.

Table 1. **^{13}C NMR shifts of H*C*=N and C≡*C*H carbons and ^{1}H NMR shifts of *H*C=N and C≡C*H* hydrogens in MEAs. Charges of C≡*C*H carbons by NBO method and dihedral angles between the aniline ring plane and the plane defined by a benzylidene ring and the C=N unit (by DFT computation)**

MEA	^{13}C NMR shift of H*C*=N [ppm]	^{1}H NMR shift of *H*C=N [ppm]	^{13}C NMR shift of C≡*C*H aniline part [ppm]	^{13}C NMR shift of C≡*C*H benzylidene part [ppm]	^{1}H NMR shift of C≡C*H* aniline part [ppm]	^{1}H NMR shift of C≡C*H* benzylidene part [ppm]	Charge of C≡*C*H aniline part	Charges of C≡*C*H benzylidene part	Dihedral angle [°]
D1	160.3	8.45	77.9	80.0	3.17	3.30	−0.213	−0.199	37.78
D2	160.6	8.45	77.9	80.0	3.17	3.30	−0.211	−0.198	39.59
D3	159.1	8.39	78.0	79.2	3.18	3.23	−0.211	−0.196	38.28
D4	160.3	8.43	77.9	78.4	3.17	3.20	−0.213	−0.203	39.17
D5	160.4	8.43	77.9	78.5	3.17	3.20	−0.211	−0.203	40.09
T1	160.1	8.52	78.0	–	3.18	–	−0.211	–	37.50
T2	159.1	8.53	–	79.9	–	3.29	–	−0.200	35.28
T3	160.5	8.50	78.1	79.2	3.18	3.27	−0.210	−0.196	38.40; 38.04
T4	157.9	8.48	–	79.1	–	3.23	–	−0.197	35.45

Characterization of MEAs

All the MEAs prepared are yellowish solids soluble in tested solvents: CH_2Cl_2, toluene, THF. The solubility of MEAs in CH_2Cl_2 at room temperature was studied in detail. The solubility of 1 mol L^{-1} was achieved for all the D-type MEAs. The solubility of T-type MEAs in CH_2Cl_2 was as follows: 0.6 mol L^{-1} (**T3**); 0.3 mol L^{-1} (**T1** and **T2**); and 0.1 mol L^{-1} (**T4**). The MEAs prepared were characterized by high-resolution mass spectrometry (HRMS), ^{1}H and ^{13}C NMR, infrared (IR) spectroscopy, and Raman spectroscopy (see Experimental).

The presence of the methanimine group in the prepared MEAs was evidenced by means of ^{1}H NMR and ^{13}C NMR spectroscopy techniques. The respective signals are in narrow intervals (δ = 8.39–8.50 ppm, *H*C=N and δ = 157.9–160.6 ppm, H*C* = N, see Table 1) regardless of the functionality, positional isomerism, and architecture of individual MEAs. The positions of the signals are close to the positions of HC=N signals in unsubstituted *N*-benzylideneaniline (δ = 8.43 ppm, *H*C=N and δ = 160.34 ppm, H*C*=N, refs[38,39]). This finding can be discussed in connection to the work of Neuvonen et al.[39] who investigated the influence of various substituents in *para* positions of *N*-benzylideneaniline rings on the ^{13}C NMR chemical shifts of carbon of the methanimine group (however, −C≡CH substituent had not been involved in this study). The authors revealed the inductive effect of the substituents as a crucial factor influencing the ^{13}C NMR chemical shifts of H*C*=N. Because the ethynyl group possesses only a low electron-withdrawing inductive effect, consequently, the ^{1}H NMR and ^{13}C NMR chemical shifts of MEAs methanimine groups are similar to those of the methanimine group of unsubstituted *N*-benzylideneaniline. The main aspect of the terminal ethynyl groups influencing electron densities is the resonance (mesomeric) effect.

The ^{13}C NMR chemical shifts and values of charges (by natural bond orbital, NBO, analysis) of terminal carbon of the ethynyl groups (C≡*C*H) are summarized in Table 1 together with the values of ^{1}H NMR chemical shifts of hydrogen of the ethynyl groups (C≡C*H*). The ^{1}H NMR signals of hydrogens of the ethynyl groups connected to the aniline part of MEAs (δ = 3.17–3.18 ppm) are slightly shifted upfield compared with the signals of hydrogens of the ethynyl groups connected to the benzylidene part of MEAs (δ = 3.20–3.30 ppm). The same conclusion results for the ^{13}C NMR signals of terminal carbon of the ethynyl groups: C≡*C*H signals of the ethynyl groups connected to the aniline part of the molecules (δ = 77.9–78.1 ppm) are shifted upfield compared with C≡*C*H signals of the ethynyl groups connected to the benzylidene part of the molecules (δ = 78.4–80.0 ppm). The influence of the *meta* or *para* positioning of the ethynyl groups (relative to the methanimine link) on the NMR shifts of their terminal hydrogen and carbon can be well followed in the D-type series of MEAs. The ^{1}H NMR (C≡C*H*) and ^{13}C NMR (C≡*C*H) chemical shifts of ethynyl groups connected to the aniline part of MEAs are not sensitive to the *meta* or *para* positional isomerism of ethynyl groups (Table 1). On the contrary, both ^{1}H NMR (C≡C*H*) and ^{13}C NMR (C≡*C*H) chemical shifts reflect the *meta* or *para* positional isomerism in the case of ethynyl groups connected to the benzylidene part of MEAs: C≡*C*H and C≡C*H* signals of the *para*-positioned ethynyls are at 80.0 and 3.30 ppm, respectively (**D1**, **D2**), whereas the corresponding signals of the *meta*-positioned ethynyls are in the intervals δ 78.4–79.2 ppm and 3.20–3.23 ppm, respectively (**D3**, **D4**, **D5**). The downfield shift of C≡*C*H and C≡C*H* signals of the *para*-positioned ethynyls may indicate that the *para*-positioned ethynyl groups are more conjugated with the benzylidene moiety than the ethynyl groups in the *meta* position(s) (see below). The observed behaviour is caused by the junction of the mesomeric effects of ethynyl and azomethine groups. The ^{13}C NMR chemical shifts of C≡*C*H carbons (ethynyl groups on both aniline and benzylidene parts of MEAs) are plotted as a function of the charge on these carbons (by NBO computation) in Fig. 1. A certain correlation between these parameters is apparent from Fig. 1. Nevertheless, besides the partial charge, other factors most probably affected the ^{13}C NMR chemical shifts of C≡*C*H carbons (e.g. the chemical neighbouring of the ethynyl group, overall geometry, and electron density of the MEA molecule).

The dihedral angle between the aniline ring plane and the plane defined by the benzylidene ring and the C=N unit is a structural parameter that is often studied in ring-substituted *N*-benzylideneanilines.[39,40] The dihedral angles obtained by DFT for the optimized ground state geometry of MEAs are given in Table 1. All the values are in a narrow range from 35.28° to 40.09°. A weak influence of the *meta* or *para* positioning of the ethynyl groups on the dihedral angle is evident in the series of

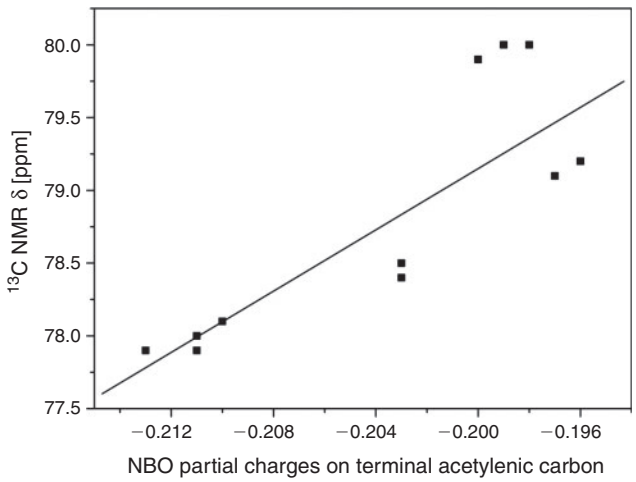

Fig. 1. ^{13}C NMR chemical shifts vs NBO partial charges for C≡*C*H carbons of MEAs.

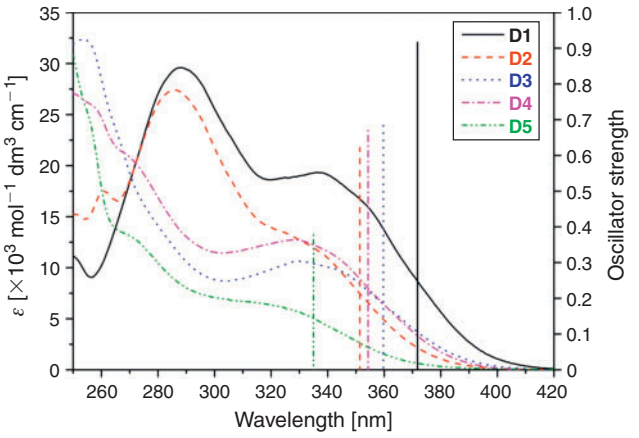

Fig. 2. UV-Visible spectra of D-type MEAs. Computed positions of HOMO–LUMO transitions are presented as perpendiculars to the wavelength axis; the length of perpendiculars is related to the oscillator strength axis.

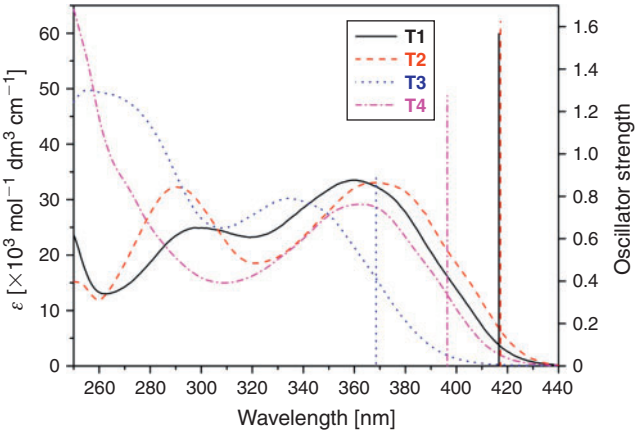

Fig. 3. UV-Visible spectra of T-type MEAs. Computed positions of HOMO–LUMO transitions are presented as perpendiculars to the wavelength axis; the length of perpendiculars is related to the oscillator strength axis.

the bifunctional D-type MEAs in which the dihedral angle increases in the order: **D1**(*pp*) < **D4**(*pm*) ≈ **D2**(*pm*) < **D5** (*mm*); letters *p* and *m* in the parentheses represent one ethynyl group in either the *para* (*p*) or *meta* (*m*) position. Evidently, each replacement of the *para*-positioned ethynyl group by the *meta*-positioned one leads to the (small) increase in the dihedral angle, most probably due to the steric effect of the *meta*-positioned ethynyl group(s). Dihedral angles of the T-type MEAs depend mainly on the composition of the MEA core. The T-type MEAs with a central ring derived from *p*-phenylenediamine exhibit dihedral angles of 35.28° (**T2**) and 35.45° (**T4**). Slightly higher dihedral angles result for the T-type MEAs with a central ring derived from benzenedicarboxaldehydes: 37.50° (**T1**); 38.04° and 38.40° (**T3**).

The Fourier transform infrared (FT-IR) and Raman spectra of MEAs are given in Figs S1 and S2 (Supplementary Material), respectively, and the representative FT-IR and Raman bands are summarized in Table S1 (Supplementary Material). Bands around 1620 cm^{-1} observed in both FT-IR and Raman spectra of all the MEAs have been ascribed to the stretching vibration of C=N bonds. The stretching vibration of NC–H bond was manifested by an FT-IR band at 2880–2900 cm^{-1}. The stretching vibration of C≡C bonds was well apparent in the Raman spectra (2100 cm^{-1}), but barely noticeable in the FT-IR spectra. The bands due to the stretching vibrations of ≡C–H bonds were observed in the FT-IR spectra only (3205–3293 cm^{-1}). An interesting phenomenon was observed in the FT-IR spectra of **D2**, **D3**, **D5**, **T3**, and **T4**. A huge difference (up to 75 cm^{-1}) was found between the positions of the FT-IR $\nu_{\equiv C-H}$ bands corresponding to individual (non-equivalent) ethynyl groups of one molecule although the positions of these bands should differ by only 2 cm^{-1} according to the DFT computation. This phenomenon could probably be caused by the Fermi resonance.

The UV-visible spectra of the MEAs are shown in Fig. 2 (D-type MEAs) and Fig. 3 (T-type MEAs). All MEAs featured spectra that contain a higher energy band and a lower energy band that correspond to the HOMO–LUMO transition and is discussed in detail. The wavelengths of the absorption maximum and low-energy edge of this band, λ_{max} and λ_{edge}, respectively, molar absorption coefficients, ε_{max}, corresponding to λ_{max}, and band gap values obtained from the edge of the UV-visible spectra are given in Table 2.

The shapes of the HOMO and LUMO orbitals of individual MEAs obtained by DFT computation are given in Fig. 4.

Table 2 and Fig. 2 clearly show that the λ_{max}, λ_{edge}, and ε_{max} values of the D-type MEAs decrease in the following order: **D1** > **D3** ≈ **D4** ≈ **D2** > **D5**. The wavelengths of the HOMO–LUMO transition computed by DFT (λ_{DFT}) as well as the values of oscillator strength exhibit the same trend (see Table 2 and Fig. 2) although all the values of λ_{DFT} are systematically red-shifted from the values of λ_{max}. The above-outlined trends show that the *meta* or *para* positioning of the ethynyl groups significantly affects the overall conjugation of the D-type MEA. The MEA with all ethynyl groups in the *meta* positions (**D5**) possesses UV-visible spectral characteristics nearly equal to those of unsubstituted *N*-benzylideneaniline (see Table 2 and compare with values for *N*-benzylideneaniline: λ_{max} = 315 nm, λ_{edge} = 370 nm, λ_{DFT} = 331 nm). Evidently, the *meta*-positioned ethynyl groups in **D5** only marginally extended the conjugation of the *N*-benzylideneaniline core. On the other hand, each replacement of the *meta*-positioned ethynyl group(s) by the *para*-positioned group leads to the red shift in the UV-visible spectrum most probably due to the extension of the conjugation of the *N*-benzylideneaniline core to the *para*-positioned ethynyl

Table 2. Characteristics of HOMO–LUMO transitions in MEAs as obtained by UV-visible spectroscopy and DFT computation

λ_{max}, absorption maximum of lower energy band ascribed to HOMO–LUMO transition; λ_{DFT}, absorption maximum of lower energy band ascribed to HOMO–LUMO transition from DFT calculation; ε_{max}, molar absorption coefficient determined from absorption maxima; λ_{edge}, absorption edge

MEA	λ_{max} [nm]	ε_{max} [$\times 10^3$ mol^{-1} dm^3 cm^{-1}]	λ_{edge} [nm]	Band gap[A] [eV]	λ_{DFT} [nm]	Oscillator strength	Band gap[B] [eV]
D1	338	19	408	3.04	371	0.917	3.76
D2	329	12	389	3.19	351	0.622	4.02
D3	331	11	395	3.12	360	0.684	3.92
D4	330	13	391	3.17	354	0.674	3.96
D5	320	6.3	366	3.38	335	0.379	4.25
T1	361	33	432	2.87	416	1.567	3.37
T2	371	33	438	2.83	417	1.625	3.44
T3	335	30	408	3.04	368	0.886	3.78
T4	364	29	428	2.89	396	1.274	3.65

[A]Obtained from the UV-vis spectra from λ_{edge}.
[B]Obtained by DFT computation.

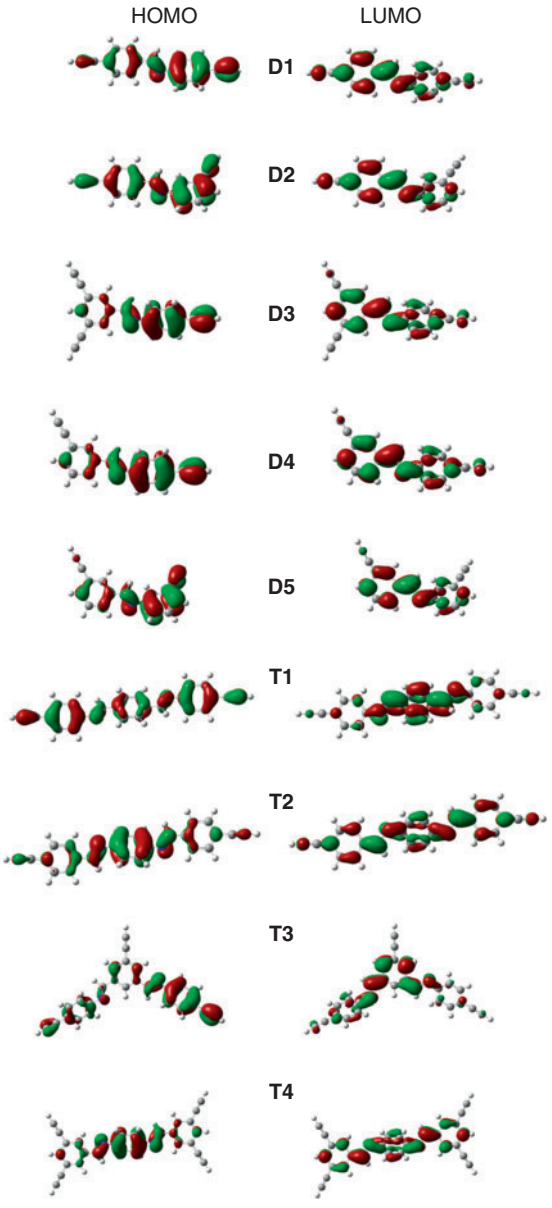

Fig. 4. Electronic density contours for LUMO and HOMO of MEAs obtained using DFT computation.

groups. Consequently, the **D1** MEA (two ethynyl groups in the *para* positions) exhibits (1) experimental λ_{max} ~18 nm red-shifted from that of **D5** and (2) ε_{max} about three times as high as that of **D5**. The finding that **D1** is the most conjugated MEA from the D-type series is consistent with the shapes of HOMO and LUMO (Fig. 4): among all the D-type MEAs, only **D1** has both HOMO and LUMO delocalized over the whole molecule including both ethynyl groups. The values of the band gap of the D-type MEAs (whether obtained from λ_{edge} or by DFT computation) are increasing with decreasing values of λ_{max}. It should be noted that DFT computation provided systematically higher values of the band gaps when compared with those obtained from the experimental UV-visible spectra (the differences are ~0.8 eV, see Table 2).

The HOMO–LUMO transitions in **T1**, **T2**, and **T4** (T-type MEAs with 1,4-phenylene central ring) are shifted to a lower energy when compared with the HOMO–LUMO transitions in the D-type MEAs (compare λ_{max}, λ_{DFT}, and band gap values of **T1**, **T2**, and **T4** with those of D-type MEAs in Table 2). This most probably reflects that the cores of **T1**, **T2**, and **T4** are one 1,4-phenylene-azomethine segment longer compared with the cores of the D-type MEAs. The UV-visible spectral characteristics of **T1**, **T2**, and **T4** exhibited only a weak influence on (1) the orientation of azomethine links between 1,4-phenylene rings (compare data for **T1** and **T2** in Table 2) and (2) *meta* or *para* positioning of ethynyl groups (compare data for **T2** and **T4** in Table 2).

As evident from Fig. 4, the HOMO and LUMO of **T1**, **T2**, and **T3** (MEAs with a 1,4-phenylene central ring) are delocalized over the whole MEA core. On the contrary, the HOMO and LUMO delocalization is interrupted on the central 1,3-phenylene ring of **T3**. This is manifested by a blue shift of the low-energy UV-visible band of **T3** in comparison with the position of this band in the spectra of **T1**, **T2**, and **T4** (see Fig. 3 and Table 2). The incorporations of 1,3-phenylene as the central ring into the T-type MEA allowed the substitution of this central ring into a sterically unhindered position 5. On the other hand, the replacement of the 1,4-phenylene central ring by the 1,3-phenylene ring led to the decrease in the conjugation extent of the T-type MEA. The DFT computation of electronic transitions in the **T3** molecule revealed that two other electronic transitions occur energetically close to the HOMO–LUMO transition ($\lambda = 360$ and 348 nm). This is most probably responsible for an apparent discrepancy between a relatively high value

of ε_{max} and a relatively low value of oscillator strength ascertained for **T3** (see Table 2).

The compounds D1and D2 exhibit photoluminescence when excited by radiation of wavelength of 340 nm. The wavelengths of the photoluminescence emission maxima, λ_{PLmax}, are 428 nm (**D1**) and 419 nm (**D2**). The photoluminescence emission spectra of **D1** and **D2** and corresponding photoluminescence lifetimes are given in Fig. S3 and Table S2 (Supplementary Material), respectively.

*Polycyclotrimerization of **D1***

The polymerizability of Schiff base-type MEAs via polycyclotrimerization was investigated with the use of the compound (monomer) **D1** and $TaCl_5/Ph_4Sn$ catalyst system. Monomer **D1** was (1) homopolycyclotrimerized according to Scheme 1 into a polyarylene-type product labelled as Pc(**D1**) and (2) copolycyclotrimerized with 1-hexyne (mole ratio in the feed, **D1**/1-hexyne = 0.5) according to Scheme 2 into a polyarylene-type product labelled as Pc(**D1**/hexyne).

The growth of the polymers proceeded via interconnecting *N*,1-bis(phenyl)methanimine cores of **D1** (labelled as **D1C**) with benzene-1,3,5-triyl and benzene-1,2,4-triyl linkers formed by [2+2+2] cyclotrimerization of ethynyl groups.[12,19] Homopolycyclotrimerization of **D1** gave insoluble (toluene, CH_2Cl_2, THF) hyperbranched Pc(**D1**) with a yield of 68 %. The elemental analysis of Pc(**D1**) provided a C/N mole ratio of 18.10 that is in good agreement with the C/N mole ratio of **D1** (C/N = 17). To reduce the degree of polymerization and to achieve a soluble product, 1-hexyne was applied as a monofunctional co-monomer for the copolycyclotrimerization with bifunctional **D1**. The copolycyclotrimerization gave Pc(**D1**/hexyne) with a yield of 62 % with respect to **D1**. The product was soluble in toluene, CH_2Cl_2, and THF although the solubility deteriorated with the Pc(**D1**/hexyne) ageing in both solid state and solution. Size

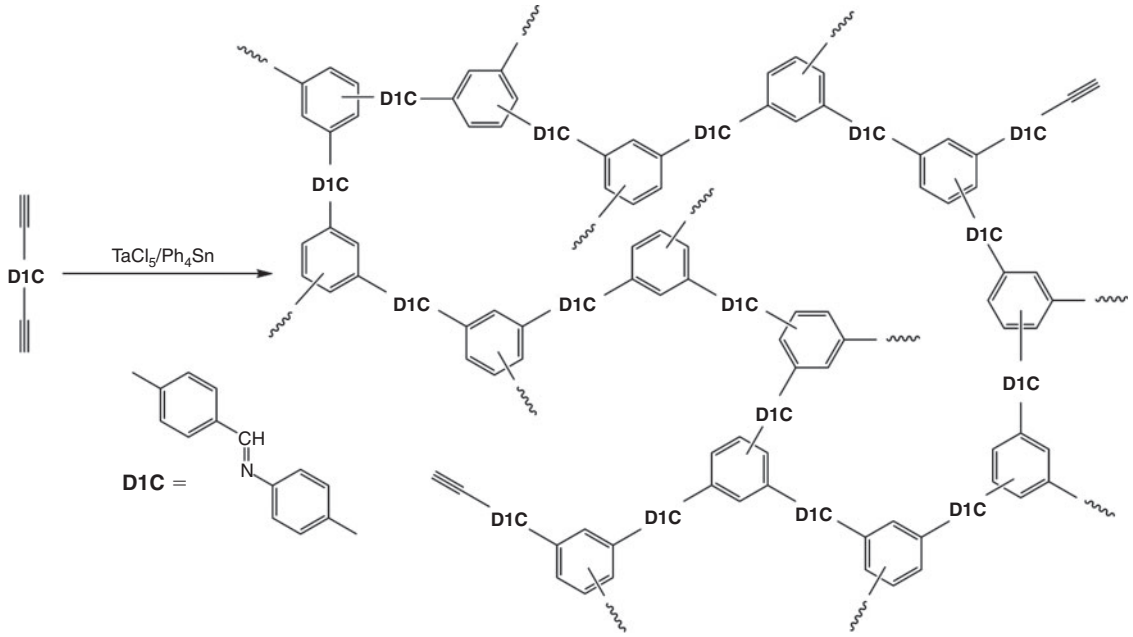

Scheme 1. Homopolycyclotrimerization of **D1**.

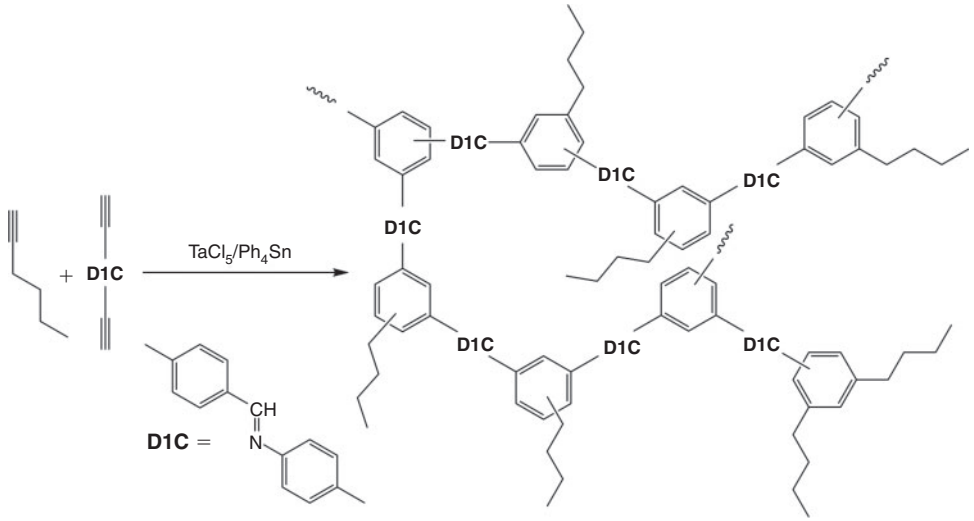

Scheme 2. Copolycyclotrimerization of **D1** with 1-hexyne.

exclusion chromatography (SEC) analysis of the freshly prepared Pc(**D1**/hexyne) provided apparent molecular weight averages, $M_w = 2000$ and $M_n = 1100$. Because the hyperbranched architecture of Pc(**D1**/hexyne) is assumed, the absolute molecular weight averages of Pc(**D1**/hexyne) are most probably higher than the apparent molecular weight averages, which are based on the calibration of SEC columns by linear polystyrene standards. The C/N mole ratio of 22.29 was determined for Pc(**D1**/hexyne), i.e. the mole ratio of monomeric units in Pc(**D1**/hexyne), $(\mathbf{D1})_{MU}/(1\text{-hexyne})_{MU}$, is 1.13. The results of elemental analysis of Pc(**D1**) and Pc(**D1**/hexyne) are given in Table S3 (Supplementary Material). Fig. 5 shows the FT-IR spectra of **D1**, Pc(**D1**), and Pc(**D1**/hexyne). The band at 1607 cm^{-1} corresponding to the stretching vibration of C=N bonds is well apparent in the spectra of both polymers. Soluble Pc(**D1**/hexyne) was characterized by ^{1}H NMR spectroscopy in CD_2Cl_2 (see Fig. S4 in Supplementary Material for the spectrum). Also, the ^{1}H NMR spectroscopy confirms the presence of the azomethine groups in the Pc(**D1**/hexyne) sample (signal region 8.4–8.7 ppm). Nevertheless, the inspection of the ^{1}H NMR spectrum also reveals a minor signal at ~10 ppm that most probably corresponds to aldehyde groups formed by partial hydrolysis of the azomethine groups. The hydrolysis may reflect the Lewis acidity of $TaCl_5$ cyclotrimerization catalyst. We have estimated the degree of hydrolysis of the CH=N groups in Pc(**D1**/hexyne) to be 25–35 % on the basis of the intensities of signals of C*H*=N and C*H*=O groups in the ^{1}H NMR spectrum. Both Pc(**D1**) and Pc(**D1**/hexyne) contain a certain amount of non-transformed ethynyl groups (see FT-IR bands corresponding to the stretching vibration of C≡C and ≡C–H bonds at 2106 cm^{-1} and 3295 cm^{-1}, respectively). The presence of ethynyl groups in Pc(**D1**/hexyne) and their slow spontaneous reaction leading to the polymer cross-linking may be responsible for the gradual deterioration of the solubility of Pc(**D1**/hexyne). The performed polycyclotrimerizations of **D1** confirmed the possibility to transform this type of MEA into hyperbranched polyarylenes with various degrees of polymerization.

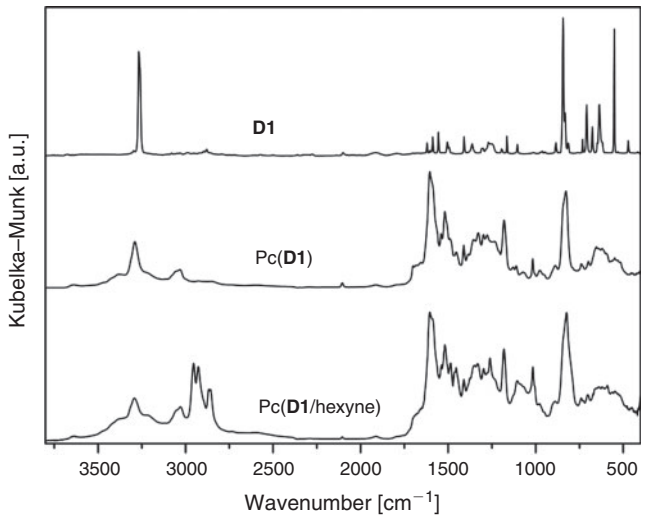

Fig. 5. FT-IR spectra of **D1**, Pc(**D1**), and Pc(**D1**/hexyne).

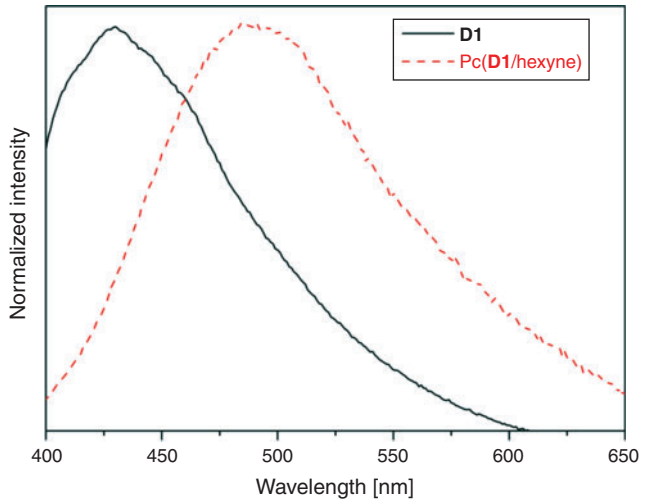

Fig. 6. Normalized photoluminescence emission spectra of **D1** (excitation wavelength: 340 nm) and Pc(**D1**/hexyne) (excitation wavelength: 350 nm).

Homopolycyclotrimer Pc(**D1**) was analyzed by nitrogen adsorption at 77 K (see Fig. S5 in Supplementary Material for the adsorption isotherm). The analysis revealed the microporous character of Pc(**D1**) with a Brunauer–Emmett–Teller surface area, S_{BET}, of 65 $m^2\,g^{-1}$. This value is lower than S_{BET} values of purely hydrocarbon microporous polyarylenes.[18,19] On the other hand, the ethynyl and methanimene groups present in Pc(**D1**) are promising for post-polymerization modification of microporous polymers of this type.[5]

The UV-visible spectrum of soluble Pc(**D1**/hexyne) (see Fig. S6 in Supplementary Material) provides the following parameters: $\lambda_{max} = 350$ nm and $\lambda_{edge} = 420$ nm. These values are slightly red-shifted from those of **D1** monomer ($\lambda_{max} = 338$ nm and $\lambda_{edge} = 408$ nm). Likewise to **D1**, Pc(**D1**/hexyne) exhibits photoluminescence when excited by radiation of a wavelength of 350 nm. The photoluminescence emission spectra of **D1** and Pc(**D1**/hexyne) and the corresponding photoluminescence lifetimes are given in Fig. 6 and Table 3, respectively.

Table 3. Photoluminescence emission characteristics of D1 and Pc(D1/hexyne)

λ_{PLmax}, wavelength of the photoluminescence emission maximum; τ_1, τ_2, and τ_3, lifetimes of the photoluminescence components (their contributions are given in parentheses)

Sample	λ_{PLmax} [nm]	Stokes shift [nm]	τ_1 [ns][C]	τ_2 [ns][C]	τ_3 [ns][C]
D1	428[A]	88	3.2 (10 %)	1.1 (52 %)	0.06 (38 %)
Pc(**D1**/hexyne)	490[B]	140	7.5 (46 %)	2.9 (44 %)	0.5 (10 %)

[A]Excitation wavelength: 340 nm.
[B]Excitation wavelength: 350 nm.
[C]Excitation wavelength: 378 nm.

Fig. 6 clearly shows that the photoluminescence emission band of Pc(**D1**/hexyne) is significantly red-shifted from that of **D1** as a result of **D1** copolycyclotrimerization. Simultaneously, the photoluminescence lifetimes of Pc(**D1**/hexyne) are significantly prolonged compared with photoluminescence lifetimes of **D1** (Table 3). Values of λ_{PLmax} of **D1** and Pc(**D1**/hexyne) are 428 nm and 490 nm, respectively, and the corresponding Stokes shifts are 88 nm in the case of **D1** and 140 nm in the case of Pc(**D1**/hexyne). Although the photoluminescent polyarylenes prepared by copolycyclotrimerization of diethynylarenes (with bulky arene cores) and 1-alkynes often exhibit large Stokes shifts, the value of 140 nm determined for Pc(**D1**/hexyne) represents an exceptionally large Stokes shift among this type of polymers.[41]

Conclusions

A series of mostly novel aromatic Schiff bases containing from two-to-four terminal ethynyl groups have been prepared. The condensation of respective amines and aldehydes, performed in a minimum amount of methanol, was used as a synthetic tool. The spectral characteristics of Schiff bases as well as the results of DFT computation are discussed in connection with the composition and architecture of the prepared compounds. The extent of conjugation depends on the size and architecture of the arene cores; mainly, the Schiff bases containing the short *N*-benzylideneaniline core exhibit a lower extent of conjugation than those with prolonged (1,4-phenylene)bis[*N*-(phenyl) methanimine] and (1,4-phenylene)bis[1-(phenyl)methanimine] cores. The extent of conjugation of the Schiff bases with a *N*-benzylideneaniline core further depends on the *meta* or *para* positioning of ethynyl groups on both benzene rings, whereby each ethynyl group in the *para* position (with respect to methanimine group) enhances the conjugation and the *meta*-positioned ethynyl groups affect the conjugation only marginally. The prepared multi-substituted Schiff bases are promising building blocks for the synthesis of conjugated polymers via polymerization of their ethynyl groups. An example is reported in which *N*,1-bis(4-ethynylphenyl)methanimine has been catalytically polycyclotrimerized into hyperbranched polyarylenes of various degrees of polymerization exhibiting either microporosity or photoluminescence.

Experimental

Materials

4-Ethynylaniline, 3-ethynylaniline, 4-ethynylbenzaldehyde, 3-ethynylbenzaldehyde, terephthalaldehyde, *p*-phenylenediamine, tantalum(V) chloride ($TaCl_5$), tetraphenyltin (Ph_4Sn), and methanol (Sigma-Aldrich), and 3,5-diethynylbenzaldehyde and 5-ethynyl-1,3-benzenedicarboxaldehyde (Spectra Group Limited, Inc.) were used as obtained. 1-Hexyne (Sigma-Aldrich) was distilled from CaH_2 under reduced pressure just before use. Toluene (Lach-Ner, Czech Rep.) was distilled from a sodium/acetophenone drying system under nitrogen just before use.

Techniques

^{1}H NMR and ^{13}C NMR measurements were performed using a Varian Unity Inova 400 spectrometer. Chemical shifts of signals in the spectra were referenced to the solvent peaks (^{1}H NMR (CD_2Cl_2, 400 MHz): $\delta = 5.32$ ppm; ^{13}C NMR (CD_2Cl_2, 101 MHz): $\delta = 54$ ppm). First-order analysis was used to evaluate all the NMR spectra received.

All FT-IR spectra were measured on a Nicolet Magna IR 760 using the diffuse reflection mode (DRIFT; diffuse reflectance infrared Fourier transform). Samples were diluted with KBr.

Raman spectra were recorded on a DXR Raman microscope (Thermo Scientific) using excitation at 780 nm and undiluted samples.

UV-visible spectra were measured in a dichloromethane solution of known concentration (10^{-5} mol dm^{-3}) on a Shimadzu PC-2401 UV-vis spectrometer.

Steady-state fluorescence was measured on a Spex 3 Jobin Yvon fluorescence spectrometer using 340 nm as an excitation wavelength. The time-resolved fluorescence decay was measured on the same apparatus using a laser (378 nm) diode as an excitation monochromator. The emission monochromator was set to luminescence maxima according to the steady-state emission spectra of the appropriate sample.

Low-resolution electron ionization mass spectra were measured on a ZAB2-SEQ double focusing mass spectrometer. Ion source conditions were as follows: electron energy, 70eV; electron current, 50 μA; and source temperature, 250°C. Accurate mass measurements were performed at a resolution of 10000 (10 % valley definition) using a peak matching technique with perfluorokerosene as the internal standard. Samples were introduced using a direct inlet probe heated up to a temperature enabling evaporation.

SEC analysis of **D1**/1-hexyne copolycyclotrimer was performed on an Agilent Technologies 1100 Series apparatus fitted with a UV-visible detector operating at 254 nm. A series of three PL-gel columns (Mixed B and Mixed C and Mixed E, Polymer Laboratories, UK) and THF as the mobile phase (flow rate 0.7 mL min^{-1}) were used. Apparent (relative to polystyrene) number-average molecular weight M_n and weight-average molecular weight M_w are reported.

Nitrogen adsorption isotherm on polycyclotrimer of **D1** was recorded at 77 K using an ASAP 2020 (Micromeritics) volumetric instrument as described elsewhere.[9]

Computation

The geometry of ground states was optimized using DFT; transition energies of absorption were calculated by time dependent-DFT using optimized ground state geometry. In all the computations, Becke's three-parameter functional with the non-local Lee–Yang–Parr correlation functional (B3LYP) with the standard 6–31G(2d,p) basis set as implemented in Gaussian was used.[42]

Synthesis of Dimer-Type MEAs

Dimers **D1**, **D2**, **D3**, **D4**, and **D5** (see below) were prepared by reaction of respective ethynyl(s)benzaldehyde (2 mmol) with respective ethynylaniline (2 mmol). Reactions were started by mixing reactant solutions (solutions were prepared by dissolving the reactants in minimum amounts of methanol, 3-ethynylaniline, which is liquid, and used undiluted). The first crystals of the product appeared in the reaction mixture within a 5–30 min interval. After 3 h, a yellowish microcrystalline precipitate was separated by filtration, washed with cold methanol to remove non-reacted starting compounds, and dried in a vacuum at room temperature to a constant weight.

Synthesis of Trimer-Type MEAs

Trimers **T1** and **T3** (see below) were prepared by reaction of respective (ethynyl)benzenedicarboxaldehyde (1 mmol) with

4-ethynylaniline (2.4 mmol). Trimers **T2** and **T4** (see below) were prepared by reaction of respective ethynyl(s)benzaldehyde (2.4 mmol) with *p*-phenylenediamine (1 mmol). Reactions were started by mixing reactant solutions (solutions were prepared by dissolving the reactants in minimum amounts of methanol). If a yellowish microcrystalline precipitate of the desired product was not formed within 3 h, the reaction mixture was cooled at −5°C to induce product crystallization. The solid product was separated by filtration, washed with cold methanol to remove non-reacted starting compounds, and dried in a vacuum at room temperature to a constant weight.

*N,1-Bis(4-ethynylphenyl)methanimine (**D1**) (Chart 2)*

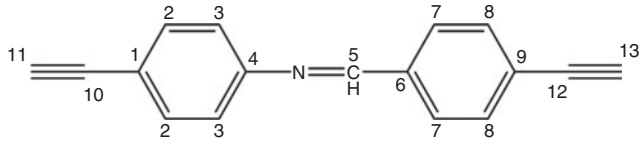

Chart 2. Structure and group numbering of **D1**.

Yield 80 %.

ν_{max} (KBr)/cm^{-1} 552s, 636m, 710m, 845*v.*, 1105vw, 1165w, 1365w, 1502w, 1556w, 1587w, 1622w, 2102w, 2881w, 3269*v.*

Raman shift (780 nm, 15 mW)/cm^{-1} 1166s, 1190w, 1556m, 1587s, 2099s.

δ_H (CD_2Cl_2, 400 MHz) 8.45 (s, 1H^5), 7.88 (d, *J* 8.3, 2H^7), 7.60 (d, *J* 8.3, 2H^2), 7.53 (d, *J* 8.5, 2H^8), 7.18 (d, *J* 8.6, 2H^3), 3.30 (s, 1H^{13}), 3.17 (s, H^{11}).

δ_C (CD_2Cl_2, 400 MHz) 160.3 (C^5), 152.7 (C^{arom}), 136.5 (C^{arom}), 133.6 (C^{arom}), 133.0 (C^{arom}), 129.3 (C^{arom}), 125.7 (C^{arom}), 121.5 (C^{arom}), 120.3 (C^{arom}), 83.9 (C^{10}), 83.6 (C^{12}), 80.0 (C^{13}), 77.9 (C^{11}).

m/z (HRMS EI) 229.0892; M$^{+\bullet}$ requires 229.0891.

*N-(3-Ethynylphenyl)-1-(4-ethynylphenyl)methanimine (**D2**) (Chart 3)*

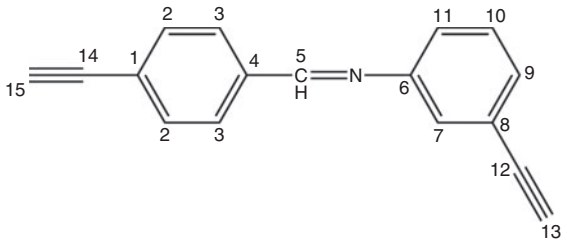

Chart 3. Structure and group numbering of **D2**.

Yield 74 %.

ν_{max} (KBr)/cm^{-1} 419m, 535m, 559m, 654s, 677*v.*, 685*v.*, 767m, 794m, 838s, 888s, 940s, 1145m, 1174m, 1211m, 1284m, 1307m, 1414m, 1476m, 1558m, 1575m, 1584m, 1602m, 1619s, 2102w, 2895w, 3221s, 3263*v.*

Raman shift (780 nm, 15 mW)/cm^{-1} 1144w, 1175m, 1211w, 1557w, 1574m, 1602s, 1621s, 2013s.

δ_H (CD_2Cl_2, 400 MHz) 8.45 (s, 1H^5), 7.88 (d, *J* 8.3, 2H^3), 7.60 (d, *J* 8.3, 2H^2), 7.37 (m, 2H^{9,11}), 7.33 (bs, 1H^7), 7.25–7.19 (m, 1H^{10}), 3.30 (s, 1H^{15}), 3.17 (s, 1H^{13}).

δ_C (CD_2Cl_2, 101 MHz) 160.6 (C^5), 152.4 (C^{arom}), 136.8 (C^{arom}), 133.0 (C^{arom}), 130.0 (C^{arom}), 129.9 (C^{arom}), 129.3 (C^{arom}), 125.7 (C^{arom}), 124.8 (C^{arom}), 123.5 (C^{arom}), 122.4 (C^{arom}), 83.7 (C^{14}), 83.6 (C^{12}), 80.0 (C^{15}), 77.9 (C^{13}).

m/z (HRMS EI) 229.0899; M$^{+\bullet}$ requires 229.0891.

*1-(3,5-Diethynylphenyl)-N-(4-ethynylphenyl) methanimine (**D3**) (Chart 4)*

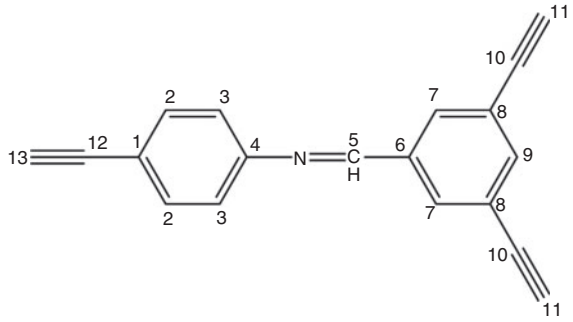

Chart 4. Structure and group numbering of **D3**.

Yield 64 %.

ν_{max} (KBr)/cm^{-1} 634s, 673s, 726w, 839s, 856m, 886s, 1501m, 1580m, 1593m, 1624m, 2104w, 2888vw, 3212*v.*, 3282*v.*

Raman shift (780 nm, 15 mW)/cm^{-1} 1144w, 1167w, 1211w, 1580s, 1594m, 1624m, 2105s.

δ_H (CD_2Cl_2, 400 MHz) 8.39 (s, 1H^5), 8.00 (d, *J* 1.5, 2H^7), 7.71 (t, *J* 1.5, 1H^9), 7.53 (d, *J* 8.5, 2H^2), 7.18 (d, *J* 8.5, 2H^3), 3.23 (s, 2H^{11}), 3.18 (s, 1H^{13}).

δ_C (CD_2Cl_2, 101 MHz) 159.1 (C^5), 152.3 C^{arom}), 138.4 (C^{arom}), 137.3 (C^{arom}), 133.8 (C^{arom}), 133.0 (C^{arom}), 123.8 (C^{arom}), 121.5 (C^{arom}), 120.6 (C^{arom}), 83.8 (C^{12}), 82.2 (C^{13}), 79.2 (C^{11}), 78.0 (C^{10}).

m/z (HRMS EI) 253.0887; M$^{+\bullet}$ requires 253.0891.

*1-(3-Ethynylphenyl)-N-(4-ethynylphenyl)methanimine (**D4**) (Chart 5)*

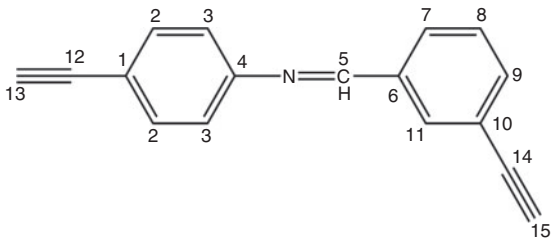

Chart 5. Structure and group numbering of **D4**.

Yield 62 %.

ν_{max} (KBr)/cm^{-1} 419m, 535m, 559m, 654s, 677*v.*, 685*v.*, 767m, 794m, 838s, 888s, 940s, 1145m, 1174m, 1211m, 1284m, 1307m, 1414m, 1476m, 1558m, 1575m, 1584m, 1602m, 1619s, 2102w, 2895w, 3221s, 3263*v.*

Raman shift (780 nm, 15 mW)/cm^{-1} 972w, 999w, 1140m, 1168w, 1365w, 1590s, 1631m, 2107m.

δ_H (CD_2Cl_2, 400 MHz) 8.43 (s, 1H^5), 8.03 (m, 1H^{11}), 7.91 (dt, J_1 7.8, J_2 1.4, 1H^7), 7.62 (dt, J_1 7.7, J_2 1.4, 2H^9), 7.54 (dm, *J* 2.2, 2H^2), 7.47 (t, *J* 7.7, 1H^8), 7.17 (dm, *J* 8.6, 2H^3), 3.20 (s, 1H^{15}), 3.17 (s, 1H^{13}).

δ_C (CD_2Cl_2, 101 MHz) 160.3 (C^5), 152.6 (C^{arom}), 136.9 (C^{arom}), 135.4 (C^{arom}), 133.7 (C^{arom}), 132.9 (C^{arom}), 129.6 (C^{arom}), 129.5 (C^{arom}), 123.4 (C^{arom}), 121.5 (C^{arom}), 120.3 (C^{arom}), 83.9 (C^{12}), 83.2 (C^{10}), 78.4 (C^{13}), 77.9 (C^{13}).

m/z (HRMS EI) 229.0888; $M^{+\bullet}$ requires 229.0891.

N,*1-Bis(3-ethynylphenyl)methanimine* (***D5***) (Chart 6)

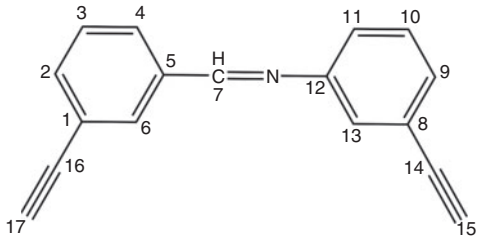

Chart 6. Structure and group numbering of **D5**.

Yield 62 %.

ν_{max} (KBr)/cm^{-1} 434m, 539m, 615s, 637s, 689*v.*, 766s, 804*v.*, 896s, 910m, 987m, 1091m, 1134s, 1224m, 1269s, 1368s, 1476s, 1567s, 1589s, 1629s, 2103m, 2918w, 3004w, 3060m, 3213s, 3280s.

Raman shift (780 nm, 15 mW)/cm^{-1} 998s, 1136s, 1224s, 1432w, 1568s, 1590s, 1628s, 2103s.

δ_H (CD_2Cl_2, 400 MHz) 8.43 (s, $1H^7$), 8.02 (t, *J* 1.6, $1H^6$), 7.91 (dt, J_1 7.8, J_2 1.4 Hz, $1H^{arom}$), 7.62 (dt, J_1 7.7, J_2 1.4, $1H^{arom}$), 7.47 (t, *J* 7.7, $1H^{arom}$), 7.41–7.35 (m, $2H^{arom}$), 7.33 (dt, J_1 2.0, J_2 1.0, $1H^{13}$), 7.25–7.19 (m, 1H), 3.20 s (s, $1H^{17}$), 3.17 (s, H^{15}).

δ_C (CD_2Cl_2, 101 MHz) 160.5 (C^7), 152.4 (C^{arom}), 136.9 (C^{arom}), 135.4 (C^{arom}), 132.9 (C^{arom}), 130.2 (C^{arom}), 129.9 (C^{arom}), 129.6 (C^{arom}), 129.5 (C^{arom}), 124.7 (C^{arom}), 123.5 (C^{arom}), 123.3 (C^{arom}), 122.4 (C^{arom}), 83.6 (C^{14}), 83.2 (C^{16}), 78.5 (C^{17}), 77.9 (C^{15}).

m/z (HRMS EI) 229.0883; $M^{+\bullet}$ requires 229.0891.

*1,1′-(1,4-Phenylene)bis[*N*-(4-ethynylphenyl) methanimine]* (***T1***) (Chart 7)

Yield 65 %.

ν_{max} (KBr)/cm^{-1} 561m, 852s, 1617w, 2104vw, 2875w, 3284s.

Raman shift (780 nm, 15 mW)/cm^{-1} 1160s, 1190w, 1556s, 1585s, 1624w, 2103m.

δ_H (CD_2Cl_2, 400 MHz) 8.52 (s, $2H^3$), 8.03 (s, $4H^1$), 7.55 (d, *J* 8.5, $4H^6$), 7.21 (d, *J* 8.5, $4H^5$), 3.18 (s, $2H^9$).

δ_C (CD_2Cl_2, 101 MHz) 160.1 (C^3), 152.7 (C^{arom}), 139.1 (C^{arom}), 133.6 (C^{arom}), 129.6 (C^{arom}), 121.6 (C^{arom}), 120.4 (C^{arom}), 83.8 (C^8), 78.0 (C^9).

m/z (HRMS EI) 332.1311; $M^{+\bullet}$ requires 332.1313.

N,N′-*(1,4-Phenylene)bis(1-(4-ethynylphenyl) methanimine)* (***T2***) (Chart 8)

Yield 83 %.

ν_{max} (KBr)/cm^{-1} 567m, 625m, 652m, 831m, 850s, 1107w, 1363m, 1616m, 2103vw, 2879w, 3288s.

Raman shift (780 nm, 15 mW)/cm^{-1} 1156m, 1171w, 1191w, 1554m, 1578s, 1604w, 2106m.

δ_H (CD_2Cl_2, 400 MHz) 8.53 (s, $2H^3$), 7.90 (d, *J* 8.3, $4H^6$), 7.61 (d, *J* 8.2, $4H^5$), 7.30 (s, $4H^1$), 3.29 (s, 2H).

δ_C (CD_2Cl_2, 101 MHz) 159.1 (C^3), 150.5 (C^{arom}), 137.4 (C^{arom}), 133.1, 128.9, 122.3, 125.3, 83.7 (C^8), 79.9 (C^9).

m/z (HRMS EI) 332.1320; $M^{+\bullet}$ requires 332.1313.

*1,1′-(5-Ethynyl-1,3-phenylene)bis[*N*-(4-ethynylphenyl) methanimine]* (***T3***) (Chart 9)

Yield 68 %.

ν_{max} (KBr)/cm^{-1} 544m, 627m, 646s, 668s, 684m, 729m, 838*v.*, 856m, 864m, 887m, 972m, 1108w, 1143m, 1157m, 1405m, 1499s, 1582s, 1596m, 1627s, 2101w, 2900w, 3205s, 3280s.

Raman shift (780 nm, 15 mW)/cm^{-1} 1141w, 1157w, 1169w, 1209w, 1308w, 1585s, 1624m, 2097m.

δ_H (CD_2Cl_2, 400 MHz) 8.50 (s, $2H^7$), 8.43 (s, $1H^6$), 8.15 (s, $2H^4$), 7.55 (d, *J* 8.5, $4H^{10}$), 7.21 (d, *J* 8.6, $4H^9$), 3.27 (s, $1H^1$), 3.18 (s, $2H^{13}$).

δ_C (CD_2Cl_2, 101 MHz) 159.5 (C^7), 152.2 (C^{arom}), 137.6 (C^{arom}), 135.3 (C^{arom}), 133.7 (C^{arom}), 129.6 (C^{arom}), 124.0 (C^{arom}), 121.6 (C^{arom}), 120.7 (C^{arom}), 83.8 (C^{12}), 82.5 (C^2), 79.2 (C^1), 78.1 (C^{13}).

m/z (HRMS EI) 356.1294; $M^{+\bullet}$ requires 356.1313.

N,N′-*(1,4-Phenylene)bis[1-(3,5-diethynylphenyl) methanimine]* (***T4***) (Chart 10)

Yield 90 %.

ν_{max} (KBr)/cm^{-1} 628s, 655m, 680s, 846s, 880s, 1498s, 1584m, 1624s, 2104w, 2885w, 3221s, 3280s.

Raman shift (780 nm, 15 mW)/cm^{-1} 1143w, 1162w, 1215w, 1288w, 1578s, 1596m, 1628m, 2109w.

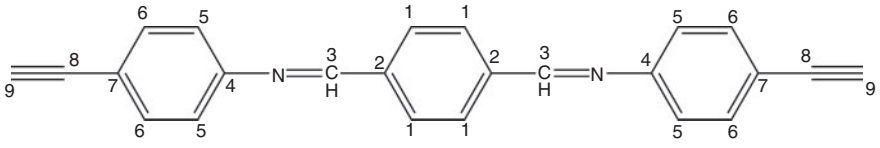

Chart 7. Structure and group numbering of **T1**.

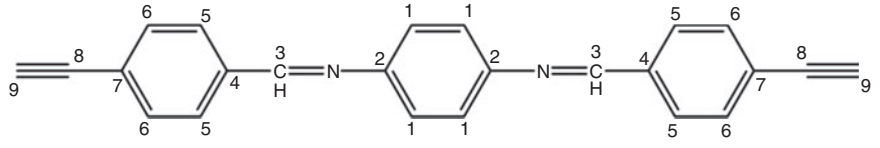

Chart 8. Structure and group numbering of **T2**.

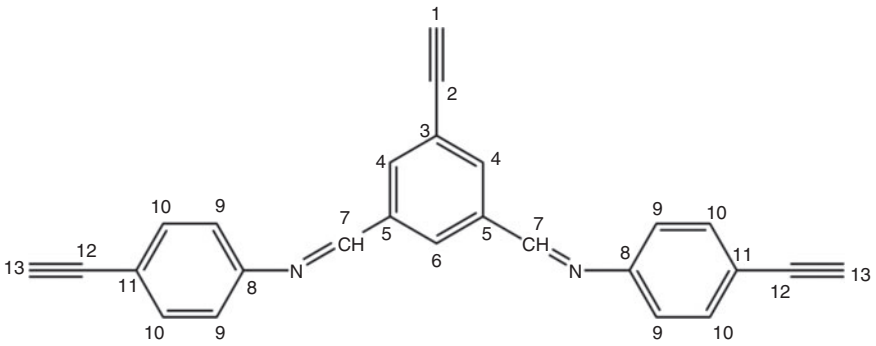

Chart 9. Structure and group numbering of **T3**.

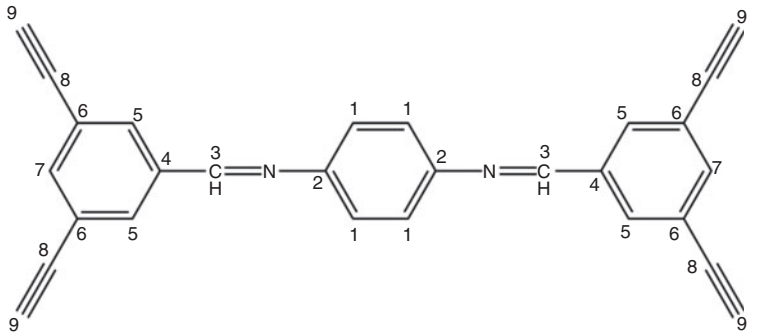

Chart 10. Structure and group numbering of **T4**.

δ_H (CD_2Cl_2, 400 MHz) 8.48 (s, 2 H^3), 8.02 (s, 4 H^5), 7.70 (s, 2 H^7), 7.30 (s, 4H^1), 3.23 (s, 4 H^9).

δ_C (CD_2Cl_2, 101 MHz) 157.9 (C^3), 150.2 (C^{arom}), 138.2 (C^{arom}), 137.5 (C^{arom}), 132.8 (C^{arom}), 123.7 (C^{arom}), 122.5 (C^{arom}), 82.3 (C^8), 79.1 (C^9).

m/*z* (HRMS EI) 380.1322; $M^{+\bullet}$ requires 380.1313.

*Homopolycyclotrimerization of **D1** and copolycyclotrimerization of **D1** with 1-Hexyne*

Polycyclotrimerizations were performed in toluene at 50°C under a nitrogen atmosphere in a drybox (PlastLabs) combined with a standard Schlenk technique. The polycyclotrimerization catalyst $TaCl_5/Ph_4Sn$ (prepared by mixing toluene solutions of $TaCl_5$ and Ph_4Sn in a round-bottom flask, equipped with a Schlenk stopper) was left to ripen for 10–15 min before use. The polycyclotrimerizations were started by mixing $TaCl_5$/Ph_4Sn and monomer(s) solutions. The initial concentrations of the reaction components in the polycyclotrimerization mixtures were $[TaCl_5]_0 = 0.015\ mol\ L^{-1}$, $[Ph_4Sn]_0 = 0.015\ mol\ L^{-1}$, $[\mathbf{D1}]_0 = 0.6\ mol\ L^{-1}$ in the case of homopolycyclotrimerization and $[TaCl_5]_0 = 0.015\ mol\ L^{-1}$, $[Ph_4Sn]_0 = 0.015\ mol\ L^{-1}$, $[\mathbf{D1}]_0 = 0.1\ mol\ L^{-1}$, $[1\text{-hexyne}]_0 = 0.2\ mol\ L^{-1}$ in the case of copolycyclotrimerization. The volume of the polycyclotrimerization mixture was 7 mL. Homopolycyclotrimerization of **D1** proceeded as a precipitation reaction. The reaction suspension was poured into excess toluene after 24 h. The solid polymer was collected, washed with toluene, and dried in a vacuum at room temperature to a constant weight. On the contrary, the polymer remained soluble in the reaction mixture in the case of copolycyclotrimerization of **D1** with 1-hexyne. The reaction solution was poured into excess methanol after 24 h. The precipitated polymer was collected, washed with methanol, and dried in a vacuum at room temperature to a constant weight. The yields of homo- and copolycyclotrimers were determined gravimetrically.

Supplementary Material

IR and Raman spectroscopic characteristics of prepared MEAs, UV-visible and luminescence spectra of Pc(D1/hexyne) and N2 adsorption isotherm on Pc(D1) are available on the Journal's website.

Acknowledgements

Financial support from the Czech Science Foundation (Project No. P108–12–1143) and the Science Foundation of Charles University (Project No. 574612 B-CH) is gratefully acknowledged. Access to computing and storage facilities owned by parties and projects contributing to the National Grid Infrastructure MetaCentrum, provided under the program 'Projects of Large Infrastructure for Research, Development, and Innovations' (LM2010005), is greatly appreciated.

References

[1] J. Z. Liu, J. W. Y. Lam, B. Z. Tang, *Chem. Rev.* **2009**, *109*, 5799. doi:10.1021/CR900149D
[2] B. Z. Tang, *Macromol. Chem. Phys.* **2008**, *209*, 1303. doi:10.1002/MACP.200800228
[3] A. C. Grimsdale, K. L. Chan, R. E. Martin, P. G. Jokisz, A. B. Holmes, *Chem. Rev.* **2009**, *109*, 897. doi:10.1021/CR000013V
[4] U. H. F. Bunz, *Adv. Polym. Sci.* **2005**, *177*, 1. doi:10.1007/B101374
[5] E. Slováková, M. Ješelnik, E. Žagar, J. Zedník, J. Sedláček, S. Kovačič, *Macromolecules* **2014**, *47*, 4864. doi:10.1021/MA501142D
[6] R. R. Hu, J. W. Y. Lam, B. Z. Tang, *Macromol. Chem. Phys.* **2013**, *214*, 175. doi:10.1002/MACP.201200389
[7] K. Seehafer, M. Bender, U. H. F. Bunz, *Macromolecules* **2014**, *47*, 922. doi:10.1021/MA402615Q

[8] R. Dawson, A. I. Cooper, D. J. Adams, *Prog. Polym. Sci.* **2012**, *37*, 530. doi:10.1016/J.PROGPOLYMSCI.2011.09.002
[9] V. Hanková, E. Slovakova, J. Zednik, J. Vohlidal, R. Sivkova, H. Balcar, A. Zukal, J. Brus, J. Sedlacek, *Macromol. Rapid Commun.* **2012**, *33*, 158. doi:10.1002/MARC.201100599
[10] R. Balamurugan, N. Naveen, S. Manojveer, M. V. Nama, *Aust. J. Chem.* **2011**, *64*, 567. doi:10.1071/CH11080
[11] U. H. F. Bunz, *Chem. Rev.* **2000**, *100*, 1605. doi:10.1021/CR990257J
[12] M. Häußler, J. Liu, J. W. Y. Lam, A. Qin, R. Zheng, B. Z. Tang, *J. Polym. Sci., Part A: Polym. Chem.* **2007**, *45*, 4249. doi:10.1002/POLA.22246
[13] X. Zhan, M. Yang, Z. Lei, *J. Mol. Catal. Chem.* **2002**, *184*, 139. doi:10.1016/S1381-1169(02)00006-7
[14] Z. Dong, Z. Ye, *Macromolecules* **2012**, *45*, 5020. doi:10.1021/MA3007569
[15] Y. Morisaki, M. Gon, Y. Chujo, *J. Polym. Sci., Part A: Polym. Chem.* **2013**, *51*, 2311. doi:10.1002/POLA.26600
[16] R. Dawson, A. Laybourn, R. Clowes, Y. Z. Khimyak, D. J. Adams, A. I. Cooper, *Macromolecules* **2009**, *42*, 8809. doi:10.1021/MA901801S
[17] J. R. Holst, E. Stöckel, D. J. Adams, A. I. Cooper, *Macromolecules* **2010**, *43*, 8531. doi:10.1021/MA101677T
[18] S. Yuan, B. Dorney, D. White, S. Kirklin, P. Zapol, L. Yu, D.-J. Liu, *Chem. Commun.* **2010**, *46*, 4547. doi:10.1039/C0CC00235F
[19] A. Zukal, E. Slovakova, H. Balcar, J. Sedlacek, *Macromol. Chem. Phys.* **2013**, *214*, 2016. doi:10.1002/MACP.201300317
[20] E. Slováková, A. Zukal, J. Brus, H. Balcar, L. Brabec, D. Bondarev, J. Sedláček, *Macromol. Chem. Phys.* **2014**, *215*, 1855. doi:10.1002/MACP.201400198
[21] Z. Wang, S. Yuan, A. Mason, B. Reprogle, D.-J. Liu, L. Yu, *Macromolecules* **2012**, *45*, 7413. doi:10.1021/MA301426E
[22] S. Ren, R. Dawson, D. J. Adams, A. I. Cooper, *Polym. Chem.* **2013**, *4*, 5585. doi:10.1039/C3PY00690E
[23] J. Wei, X. Zhang, Y. Zhao, R. Li, *Macromol. Chem. Phys.* **2013**, *214*, 2232.
[24] R. Dawson, A. I. Cooper, D. J. Adams, *Polym. Int.* **2013**, *62*, 345. doi:10.1002/PI.4407
[25] S. Qiao, Z. Du, C. Yang, Y. Zhou, D. Zhu, J. Wang, X. Chen, R. Yang, *Polymer* **2014**, *55*, 1177. doi:10.1016/J.POLYMER.2014.01.029
[26] J.-X. Jiang, C. Wang, A. Laybourn, T. Hasell, R. Clowes, Y. Z. Khimyak, J. Xiao, S. J. Higgins, D. J. Adams, A. I. Cooper, *Angew. Chem., Int. Ed.* **2011**, *50*, 1072. doi:10.1002/ANIE.201005864
[27] M. Häußler, A. Qin, B. Z. Tang, *Polymer* **2007**, *48*, 6181. doi:10.1016/J.POLYMER.2007.08.044
[28] O. Lavastre, I. Illitchev, G. Jegou, P. H. Dixneuf, *J. Am. Chem. Soc.* **2002**, *124*, 5278. doi:10.1021/JA025764O
[29] W. Qin, S. Long, M. Panunzio, S. Biondi, *Molecules* **2013**, *18*, 12264. doi:10.3390/MOLECULES181012264
[30] Y. Wei, R. Hariharan, J. K. Ray, *J. Polym. Sci., Part A: Polym. Chem.* **1991**, *29*, 749. doi:10.1002/POLA.1991.080290517
[31] J. P. Armistead, T. M. Keller, S. B. Sastri, *Carbon* **1994**, *32*, 345. doi:10.1016/0008-6223(94)90198-8
[32] I. R. Whittall, M. G. Humphrey, A. Persoons, S. Houbrechts, *Organometallics* **1996**, *15*, 1935. doi:10.1021/OM950487Y
[33] H. Balcar, J. Čejka, J. Kubišta, L. Petrusová, P. Kubát, V. Blechta, *Collect. Czech. Chem. Commun.* **2000**, *65*, 203. doi:10.1135/CCCC20000203
[34] H. Balcar, J. Sedláček, J. Vohlídal, J. Zedník, V. Blechta, *Macromol. Chem. Phys.* **1999**, *200*, 2591. doi:10.1002/(SICI)1521-3935(19991201)200:12<2591::AID-MACP2591>3.0.CO;2-N
[35] H. Balcar, J. Sedláček, J. Zedník, V. Blechta, P. Kubát, J. Vohlídal, *Polymer* **2001**, *42*, 6709. doi:10.1016/S0032-3861(01)00148-3
[36] S. M. A. Karim, R. Nomura, T. Masuda, *Polym. Bull.* **1999**, *43*, 305. doi:10.1007/S002890050615
[37] Y. Zhang, K. Gao, Z. Zhao, D. Yue, Y. Hu, T. Masuda, *J. Polym. Sci., Part A: Polym. Chem.* **2013**, *51*, 5248. doi:10.1002/POLA.26955
[38] http://sdbs.riodb.aist.go.jp/sdbs/cgi-bin/cre_index.cgi (accessed October **2014**).
[39] H. Neuvonen, K. Neuvonen, F. Fülöp, *J. Org. Chem.* **2006**, *71*, 3141. doi:10.1021/JO0600508
[40] V. Proks, M. Holík, *Collect. Czech. Chem. Commun.* **2004**, *69*, 1566. doi:10.1135/CCCC20041566
[41] H. Peng, J. W. Y. Lam, B. Z. Tang, *Polymer* **2005**, *46*, 5746. doi:10.1016/J.POLYMER.2005.05.039
[42] M. J. Frisch, G. W. Trucks, H. B. Schlegel, G. E. Scuseria, M. A. Robb, J. R. Cheeseman, G. Scalmani, V. Barone, B. Mennucci, G. A. Petersson, H. Nakatsuji, M. Caricato, X. Li, H. P. Hratchian, A. F. Izmaylov, J. Bloino, G. Zheng, J. L. Sonnenberg, M. Hada, M. Ehara, K. Toyota, R. Fukuda, J. Hasegawa, M. Ishida, T. Nakajima, Y. Honda, O. Kitao, H. Nakai, T. Vreven, J. A. Montgomery, J. E. Peralta, F. Ogliaro, M. Bearpark, J. J. Heyd, E. Brothers, K. N. Kudin, V. N. Staroverov, R. Kobayashi, J. Normand, K. Raghavachari, A. Rendell, J. C. Burant, S. S. Iyengar, J. Tomasi, M. Cossi, N. Rega, J. M. Millam, M. Klene, J. E. Knox, J. B. Cross, V. Bakken, C. Adamo, J. Jaramillo, R. Gomperts, R. E. Stratmann, O. Yazyev, A. J. Austin, R. Cammi, C. Pomelli, J. W. Ochterski, R. L. Martin, K. Morokuma, V. G. Zakrzewski, G. A. Voth, P. Salvador, J. J. Dannenberg, S. Dapprich, A. D. Daniels, O. Farkas, J. B. Foresman, J. V. Ortiz, J. Cioslowski, D. J. Fox, *Gaussian 09, Revision D.01* **2013** (Gaussian, Inc.: Wallingford, CT).